Theoretical investigation of the electronic properties of potassium graphite

D. P. DiVincenzo and S. Rabii
Department of Electrical Engineering and Science, Moore School of Electrical Engineering, University of Pennsylvania, Philadelphia, Pennsylvania 19104
(Received 31 August 1981)

We present the results of a band-structure calculation for the first-stage graphite-intercalation compound of potassium, KC_8. A modified Korringa-Kohn-Rostoker formalism which was applied successfully to LiC_6 has been used. To good approximation, the KC_8 bands are given by those of two-dimensional graphite folded into the smaller Brillouin zone of KC_8, with $\frac{1}{8}$ of an extra electron per C atom. The K $3p$ states lead to a dispersionless set of bands 14 eV below the Fermi level, and the K $4s$ states create an isotropic, parabolic band with a minimum 1.8 eV above E_F. Hybridization of K states with the filled C bands is fairly weak but has a noticeable effect on the band dispersion at the Fermi level. From our band calculation we extract the KC_8 density of states, the Fermi surface, de Haas–van Alphen frequencies and masses, and plasma frequencies. We find fairly good agreement with the experimental de Haas–van Alphen frequencies, but our calculated density of states at the Fermi level is smaller than that obtained from low-temperature specific heat. We compare our work with other experimental and theoretical studies of KC_8.

I. INTRODUCTION

The intercalation compounds of graphite are highly anisotropic metals which consist of a regular array of n carbon planes separating planes of some foreign species (e.g., Li, K, AsF_5, $SbCl_5$, Br_2), n denoting the stage of the compound. These compounds have been the object of great experimental and theoretical interest in recent years[1–4] because of the tremendous chemical variety they offer, because of the different ordered phases which they display, and because of the unique competition in their binding properties between covalent, metallic, and electrostatic.

This paper presents the results of a band-structure calculation for the saturated intercalation compound of potassium, first-stage potassium graphite, KC_8. We have been motivated by the successful earlier calculation for first-stage lithium graphite, LiC_6,[5] by the availability of other theoretical studies[6,7] of KC_8, and by the question of the degree of occupancy of the K s band. By applying the identical modified Korringa-Kohn-Rostoker (KKR) formalism to KC_8 as was used for LiC_6, we hope to follow the chemical and structural trends for different members of the alkali metals and to provide a further test of the formalism. KC_8 has the additional advantage that, besides LiC_6, it is structurally one of the simplest and best characterized intercalation compounds. Also, KC_8 has been particularly well studied by a variety of experimental techniques. Many of these experiments have been interpreted in terms of the previous theoretical band-structure calculations[6,7] on KC_8. We will provide a thorough reexamination of these measurements in light of the present work.

The remainder of our paper is organized as follows. Section II discusses the crystal structure and symmetry of KC_8 and the model one-electron potential which we use. Section III presents the non-muffin-tin KKR formalism for the band-structure calculation. The energy bands of KC_8 are shown in Sec. IV, and Sec. V gives the KC_8 density of states, Fermi surface, plasma frequencies, and de Haas–van Alphen frequencies and masses. Section VI discusses our results in terms of a number of the experiments on KC_8.

II. CRYSTAL STRUCTURE AND POTENTIAL

The crystal structure of KC_8, shown in Fig. 1, has been firmly established by experiment.[8,9] It consists of alternate layers of potassium and car-

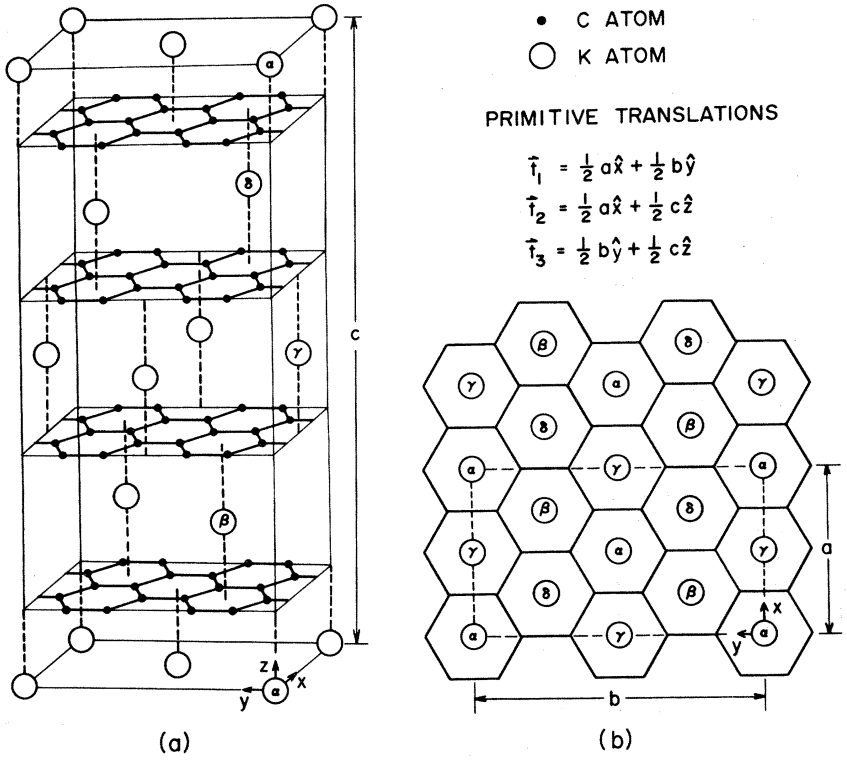

FIG. 1 (a) Conventional face-centered orthorhombic unit cell for KC_8. (b) Top view of the KC_8 structure.

bon. The carbon layers form an open hexagonal net as in pure graphite; the nearest-neighbor carbon-carbon separation is 1.42 Å. Adjacent carbon layers are in registry (*A-A* stacking) and are separated by 5.35 Å. K layers order in a triangular lattice such that a potassium atom lies above the center of every fourth carbon hexagon; that is, the potassium atoms form a 2×2 superlattice. Adjacent K layers are staggered, and begin successively at each of four possible origins denoted α, β, γ, and δ. Thus the intercalant layer sequence follows the pattern $\alpha\beta\gamma\delta\alpha\beta\gamma\delta\alpha\ldots$.

The space-group symmetry of KC_8 is *Fddd* (C_{2h}^{24}).[10,11] The Bravais-lattice type is face-centered orthorhombic. Figure 1 outlines the conventional orthorhombic unit cell, which contains four primitive unit cells. Besides translational symmetry operations, there are eight operations which leave the crystal invariant: identity, three orthogonal twofold rotations through a potassium atom, inversion, and three distinct diamond-type glide planes. The point group about each K site is 222 (D_2), and about each C site it is 1 (E), the trivial group. Each primitive unit cell contains two K atoms and 16 C atoms. The two K atoms are equivalent by symmetry. However, there are two crystallographically distinct C atoms; half of the carbons have two potassium nearest neighbors, the other half only one. All of this symmetry information is indispensable for the accurate calculation of wave functions and matrix elements (Appendix C).

The one-electron model potential is constructed by the superposition of spherically averaged atomic-charge densities for K and C. Slater's $X\alpha$ approximation to the exchange and correlation[12] is used, with Schwarz's[13] values of $\alpha=0.721\,17$ for K and $\alpha=0.759\,28$ for C. Atomic calculations are carried out using the Hartree-Fock-Slater self-consistent-field technique as developed by Herman and Skillman.[14] We use the following atomic configurations:

$$C(-\tfrac{1}{8}):\ 1s^2 2s^1 2p^{3+1/8}\ ,$$

$$K(+1):\ 1s^2 2s^2 2p^6 3s^2 3p^6\ .$$

These reflect the known sp^2 hybridization of the σ bonding states of carbon and the presumed ionization of the potassium intercalant in the crystal.

III. FORMALISM

The large anisotropy of KC_8 dictates the technique which we use to solve Schrödinger's equation

for our model potential. Figure 2 shows the crystal potential at carbon and potassium sites along several directions. Even within the C and K atomic spheres this potential is highly nonspherical, and it is far from flat in the interstitial region. This discourages the use of a conventional muffin-tin (MT) approximation. We have modified the standard muffin-tin formulation of the KKR technique[15,16] to accurately calculate the eigenstates and eigenvalues of such a system. Our method, applied recently to LiC_6 (Ref. 5) and developed originally by Painter,[17] still relies on the separation of the crystal volume into muffin-tin and interstitial regions. In KC_8 the carbon muffin-tin (CMT) spheres are chosen to touch ($r_{\mathrm{CMT}}=0.71$ Å), then the potassium muffin-tin (KMT) spheres are required to touch to carbon muffin tins ($r_{\mathrm{KMT}}=2.34$ Å). The muffin tins contain 58% of the crystal volume. The crystal potential is then divided into two parts: $V_{\mathrm{cryst}}(\vec{r})=V_{\mathrm{MT}}(\vec{r})+\Delta V(\vec{r})$. $V_{\mathrm{MT}}(\vec{r})$ is the full potential inside the muffin tins, a constant ($V_I=-0.984$ Ry) in the interstitial volume. The eigenvalues and eigenvectors for the muffin-tin part of the potential $V_{\mathrm{MT}}(r)$ are obtained from a KKR secular equation:

$$\sum_{\tau',l',m'}[\mathcal{K}^{-1}(E)^{\vec{\tau}}_{lml'm}\delta_{\vec{\tau}\vec{\tau}'}+M(\vec{k},E)^{\vec{\tau}\vec{\tau}'}_{lml'm'}]\times w(\vec{k},E)^{\vec{\tau}}_{l'm'}=0\ . \quad (1)$$

$\mathcal{K}^{-1\,\vec{\tau}}_{lml'm'}$ is the inverse scattering matrix, $M^{\vec{\tau}\vec{\tau}'}_{lml'm'}$ is the structure factor matrix, $\vec{\tau}$ and $\vec{\tau}'$ index atoms in the unit cell, l,m,l',m' are angular momentum indices, and the $w^{\vec{\tau}}_{lm}$'s are the components of the KKR eigenfunction. Appendix A describes the details of this calculation. The energies and wave functions obtained from Eq. (1), E_{KKR} and $\Psi^{\mathrm{KKR}}_n(\vec{k},\vec{r})$, are then used in a second secular equation, which takes the remainder of the crystal potential $\Delta V(\vec{r})$ into account:

$$\sum_m[(E_{\mathrm{KKR}}-E_{\mathrm{final}})\delta_{mn}+\Delta_{mn}(\vec{k})]C_m(\vec{k})=0\ , \quad (2)$$

where $\Delta_{mn}(\vec{k})$ is the matrix element of $\Delta V(\vec{r})$ between the KKR wave functions:

$$\Delta_{mn}(\vec{k})=\int_{\substack{\mathrm{unit}\\ \mathrm{cell}}}\Psi^{*\mathrm{KKR}}_m(\vec{k},\vec{r})\Delta V(\vec{r})\Psi^{\mathrm{KKR}}_n(\vec{k},\vec{r})d\vec{r}\ . \quad (3)$$

Appendix B explains in detail the calculation of the KKR wave functions and the numerical methods used for the integral in Eq. (3). Diagonal-

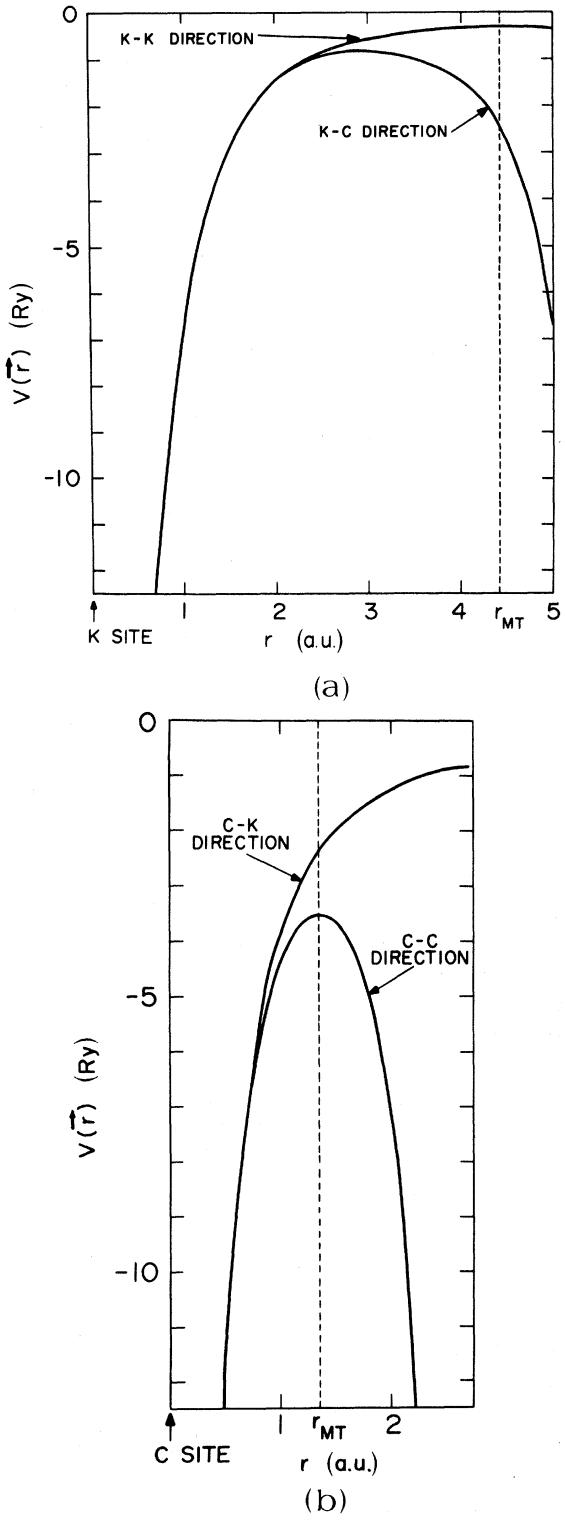

FIG. 2. Model one-electron crystal potential for KC_8 (a) around the K atom in different nearest-neighbor directions, and (b) around the C atom in different nearest-neighbor directions. The muffin-tin radii are indicated.

ization of Eq. (2) gives the final energy bands and eigenfunctions for this calculation.

IV. CALCULATED ENERGY BANDS

Equations (1)—(3) of Sec. III allow us to find the energy eigenvalues $E(\vec{k})$ for any wave vector in the Brillouin zone. In the present calculation we have determined the bands in a 40-eV energy range at the high-symmetry $\vec{k}$ points Γ, X, Y, and Z, and along the high-symmetry directions Σ, Δ, A, and B—14 points in all, as shown in Fig. 3.

Figure 4 shows the resulting band structure for KC_8. The bands are labeled according to the irreducible representation of the group of $\vec{k}$.[18] Except for the set of dispersionless K $3p$ bands at -18.9 eV, the bands drawn as solid lines up to an energy of about -10.5 eV come from the $\sigma(sp^2)$ states of graphite. Up to an energy of about -5 eV, bands derived from the π bands of graphite are dashed; above this energy, the π bands mix too much with other states to be distinguished clearly. On this band structure, the Fermi energy of graphite lies at approximately -6.8 eV.

Many of the KC_8 energy bands at and below the Fermi level can be identified with the π and σ bands of two-dimensional graphite. This identification is made clear by comparing our calculation with the KC_8 bands in the "folded-band" approximation, in which we assume that there is no interaction between the carbon layers and that the K potential is vanishingly small at the graphite planes. Under these conditions the KC_8 bands have no k_z dispersion and are simply given by the bands of two-dimensional graphite folded into the KC_8 Brillouin zone; Fig. 5 shows the result of such folding applied to Nagayoshi's[19] graphite bands. (The zeros of energy in Figs. 4 and 5 are not related.) Comparing this with our calculated KC_8 bands shows the σ band shapes to be quite similar to those of the folded bands. The 16-eV width of the σ bands is correctly predicted by Fig. 5, and the band degeneracies indicated on the folded bands correspond in each case to the same number of nearly degenerate bands in Fig. 4.

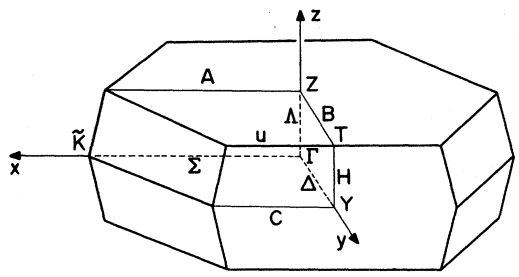

FIG. 3. Brillouin zone of KC_8. Special points and lines are labeled according to Ref. 18.

A closer comparison of the KC_8 bands with the folded two-dimensional graphite levels also reveals important differences. While the lowest-energy π bands of KC_8 have the same shape as those of graphite, the position of the π bands relative to the σ bands is about 2 eV lower than in graphite. This is consistent with the expectation that the energy of the π states, which extend away from the carbon layer, will be lowered by the attractive potassium potential. Around the Fermi level, the presence of potassium also has a significant effect on the π band shapes, and the splittings of degenerate graphite levels are greater than 1 eV. The effective masses of the π bands starting as Γ_1^+ and Γ_2^+ states at about -5.1 eV are reversed from negative to positive by the interaction with potassium states. For energies higher than -4 eV, the picture of the KC_8 bands as slightly perturbed graphite states breaks down completely.

Besides disturbing the carbon eigenstates, potassium introduces entirely new bands which originate from K atomic levels. The core $3p$ states of potassium manifest themselves as a set of six almost flat bands at -19 eV. Although they lie within the σ bands, they interact very little with the carbon planes and remain corelike. The valence $4s$ level of potassium appears as a parabolic band with its minimum, Γ_1^+ at -3.5 eV, about 1.8 eV above the Fermi level. The band starting at the Γ_1^- level at -2.9 eV is another piece of the K $4s$ band arising from folding in the k_z direction. Although these bands interact significantly with graphite levels, particularly along the Σ direction, they largely retain their K s identity throughout the Brillouin zone. In contrast to the graphite state, the K $4s$ bands have significant dispersion in the k_z direction, which is consistent with their metallic, isotropic, plane-wave character.

V. FERMI-LEVEL PROPERTIES

In order to obtain the shape of the Fermi surface and calculate the optical properties of KC_8, we need to know the energy bands on a fine mesh in the Brillouin zone. It is, however, not feasible to use an *ab initio* approach for this purpose. Therefore, we have fitted a tight-binding model to our

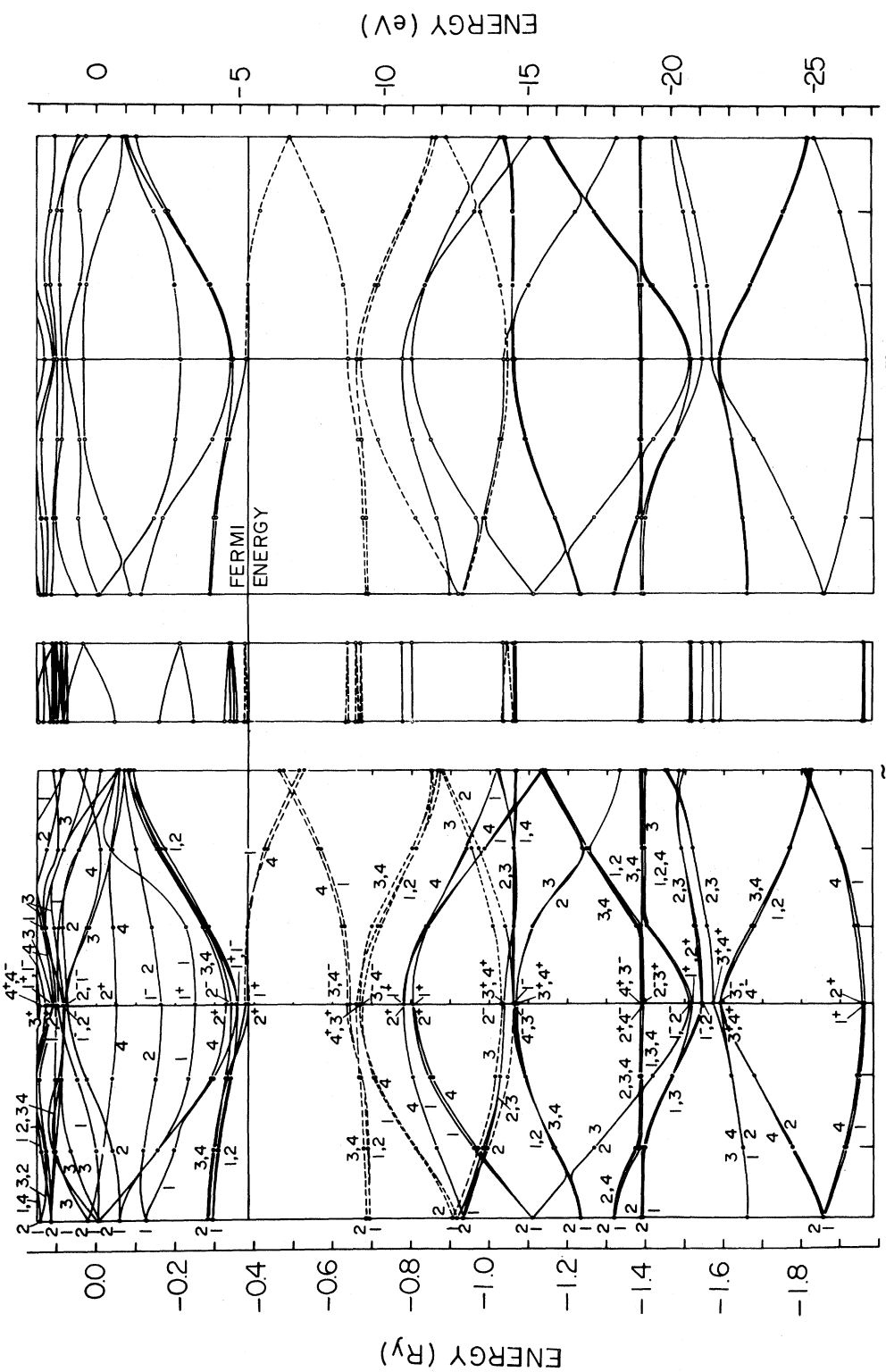

FIG. 4. Energy-band structure for KC_8 along several high-symmetry directions in the Brillouin zone. Bands drawn solid correspond to predominantly σ graphite states, except for the K $3p$ levels at -18.9 eV. Bands derived from the π states of graphite are shown dashed up to -5 eV. The minimum of the K $4s$ band is the Γ_1^+ state at -3 eV.

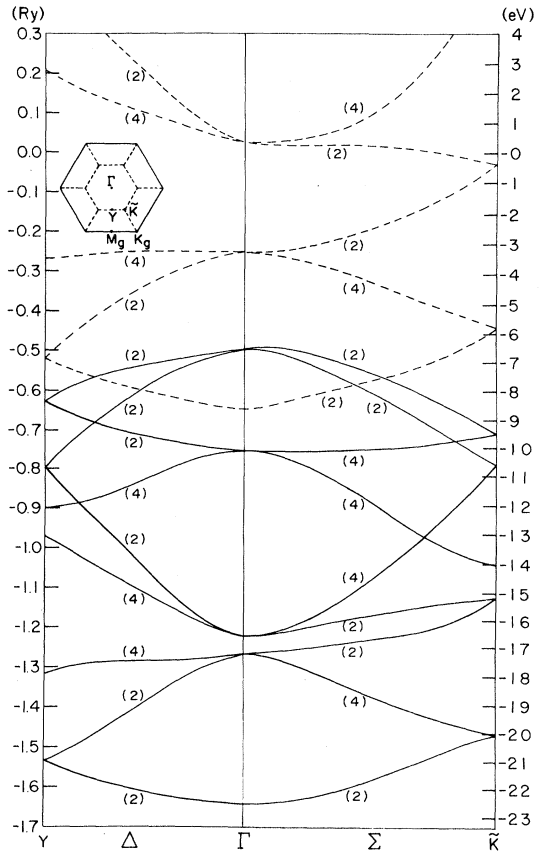

FIG. 5. Energy bands of two-dimensional graphite (Ref. 19) folded into the smaller Brillouin zone of two-dimensional KC_8. σ bands are solid lines, π band dashed. The inset shows the relationship between the graphite and KC_8 zones.

KKR results. This model uses C π and K s orbitals and includes first-, second-, and third-neighbor interactions between in-plane carbons, one carbon-carbon interplane interaction, nearest-neighbor C-K interactions, and first- and second-neighbor K-K interactions. The two-center approximation is used in this calculation.[20] These matrix elements (13 in all) were adjusted to minimize the disagreement with the *ab initio* KKR calculation near the Fermi level. The resulting fit matched all the C π bands and K s bands to within 0.3 eV, and agreed with the KKR bands in the vicinity of the Fermi energy to within 0.005 eV.

The simplicity of this linear combination of atomic orbitals (LCAO) model allows us to accurately determine the KC_8 density of states, Fig. 6. This calculation uses the histogram method to do the density sum on 31 004 points in the Brillouin zone, with an energy resolution of 0.06 eV. This

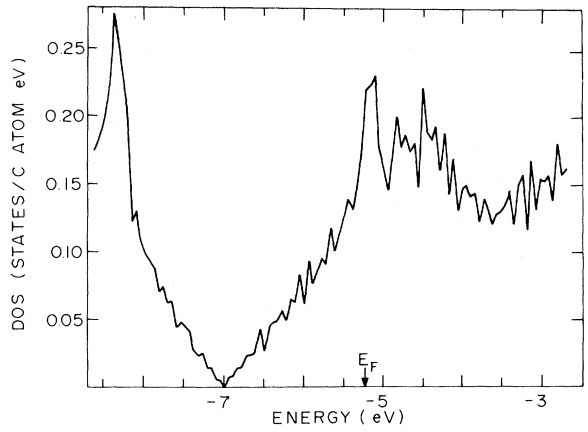

FIG. 6. Density of states of KC_8 as determined by an LCAO fit to the first-principles energy bands (Fig. 4).

density of states is very similar to that of pure graphite[21] with the band minimum at -6.9 eV and the peaks due to the saddle points at M at -8.6 and -5.0 eV. The K 4s band shows a sharp onset in the density of states at about -3.0 eV. By integrating this density of states, we determine the Fermi level shown, $E_F = -5.23$ eV. This lies about 1.4 eV above the graphite Fermi level, near the upper M point peak in the density of states. The 4s metal band lies about 1.8 eV above E_F. According to this calculation, the density of states at the Fermi energy is 0.2 states/C atom eV; the value observed from specific-heat measurements[22] is 0.33 states/C atom eV. We will examine this discrepancy in Sec. IV. We have also used the LCAO fit to the KC_8 bands to calculate the Fermi surface, shown in Fig. 7. The surface consists of two electron sheets centered at each of the six corners of the Brillouin zone. The sheets are roughly triangular and show rather small dispersion in the k_z direction, in reasonable agreement with the Fermi surface in the two-dimensional rigid-band model.[5] Even though the metal band is completely empty in our calculation, there is the possibility of a third pocket of the Fermi surface centered at the Γ point in the Brillouin zone resulting from the distortion of the π bands caused by interaction with K s band. To within the accuracy of our calculation, the Γ_2^+ level is degenerate with the Fermi level; therefore, our calculation is unable to determine whether that portion of the C π band will contribute a Fermi-surface pocket, or how large it will be. We can establish bounds on the size of the sheet: Taking the overall accuracy of our calculation to be 0.1 eV, this portion of the

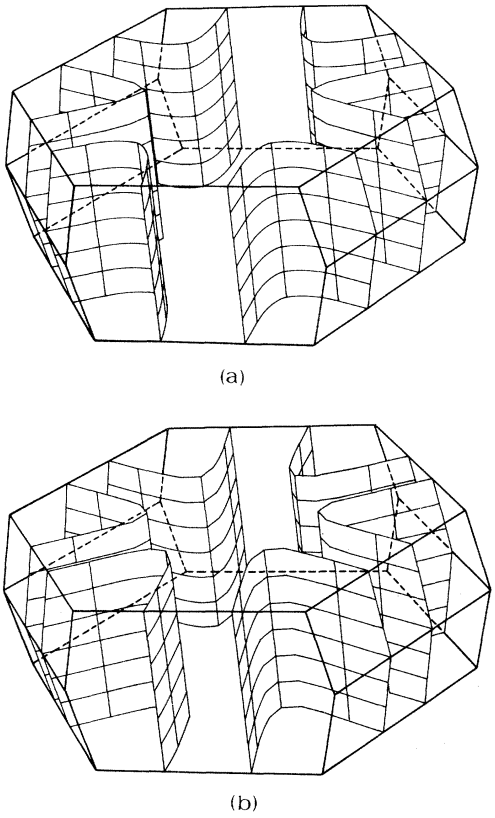

FIG. 7. (a) Lower and (b) upper band Fermi surfaces of KC_8 as derived from our LCAO interpolation of the KC_8 bands.

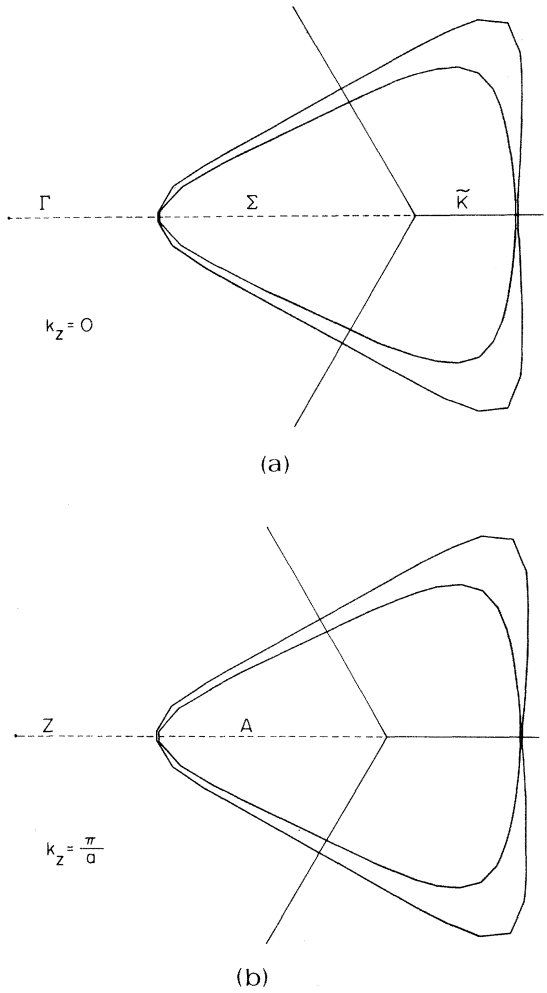

FIG. 8. Extremal cross sections of the Fermi surfaces in the (a) $k_z=0$ plane and (b) in the $k_z=\pi/c$ plane.

Fermi surface will be spheroidal and will contain no more than 0.06 electrons. In the present calculation, it is unlikely that this pocket of the Fermi surface will connect to the other sheets centered at the corners of the Brillouin zone. The presence or absence of this portion of the Fermi surface could have observable effects, as we shall discuss later.

Figure 8 shows the extremal cross sections of the Fermi surface normal to the k_z direction. There are two orbits in the $k_z=0$ plane and two in the $k_z=\pi/c$ plane. These orbits do not have trigonal symmetry as predicted by the rigid-band model because of the details of the three-dimensional stacking of the K layers (i.e., the fact that the crystal structure is orthorhombic rather than hexagonal). For each of these orbits, we can calculate the de Haas–van Alphen frequencies and masses.[5,23] As shown in Table I, these frequencies are very close together, reflecting the two dimensionality of the Fermi surface. These frequencies compare fairly well with the single observed de Haas–van Alphen frequency in KC_8, 2.9×10^7 G.[24]

The partly filled Cπ band makes an intraband contribution to the dielectric tensor, which for infinite lifetime carriers is of the form

$$\epsilon_{ij}(\omega)=1+\frac{(\omega_{ij})^2}{\omega^2}\ . \tag{4}$$

The plasma-frequency tensor is given by an integral over the Fermi surface.[25] Because of the orthorhombic symmetry of KC_8, the plasma frequency has three independent components ω_{xx}, ω_{yy}, and ω_{zz}. Measurements on highly oriented pyrolitic graphite (HOPG) intercalation compounds are only capable of measuring two components: $\omega_c=\omega_{zz}$ and $\omega_a^2=\frac{1}{2}(\omega_{xx}^2+\omega_{yy}^2)$. We have calculated all of these and show them in Table I. The anisotropy of the plasma frequency is very large, $\omega_a/\omega_c\simeq10^4$. Although the exact value of this ra-

TABLE I. Calculated Fermi-level density of states, plasma frequencies, and de Haas–van Alphen frequencies and masses for KC_8.

	Lower band	Upper band	Total
$N(E_F)$ (states/C atom eV)			0.2
ω_{xx} (eV)	3.0	3.0	4.3
ω_{yy} (eV)	3.2	3.5	4.7
$\omega_{zz}=\omega_c$ (meV)	0.27	0.10	0.29
ω_a (eV)	3.1	3.3	4.5
dHvA frequencies (G)			
$k_z=0$ plane	3.7×10^7	4.7×10^7	
$k_z=\pi/c$ plane	3.7×10^7	4.7×10^7	
dHvA masses (me)			
$k_z=0$ plane	0.58	0.70	
$k_z=\pi/c$ plane	0.58	0.70	

tio cannot be determined with great precision by our LCAO fit, it is certainly much greater than the value $\omega_a/\omega_c\simeq8$ which Zanini and Fischer[26] have derived from polarized reflectance measurements.

VI. DISCUSSION AND CONCLUSIONS

Many recent experiments on KC_8 have been interpreted using the calculated band structure of Inoshita *et al.*[6] and Ohno *et al.*[7] A comparison of the results of the present study with their results shows that although the positions of the bands near the Fermi level generally agree to within about 0.5 eV, nevertheless the Fermi surfaces are topologically quite different. In particular, the earlier work has a Fermi surface containing both cylindrical pieces at the zone corners and spherical pieces at the zone center, and these pieces are partially connected. The present studying contains cylindrical parts with at most a very small, isolated pocket at Γ.

Several of the experiments on KC_8 suggest that states at the Fermi energy have K s character. We caution, however, that having K s states at the Fermi level could result either from a partially filled metal band or hybridization of metal s states with the C π bands near E_F. Many experiments which are capable of detecting deviations from rigid-band behavior cannot distinguish between these possibilities. With this in mind, we now review the experimental data and their interpretation in light of the present calculation.

The density of states at the Fermi energy as determined by low-temperature specific-heat measurements[22] is, as mentioned earlier, substantially higher that what we predict. Inoshita *et al.*'s calculated result, $N(E_F)=0.27$ states/C atom eV is significantly closer to the measured value, although the discrepancy is still substantial. An attempt to account for this discrepancy by a specific-heat enhancement from the electron-phonon interaction was unsuccessful.[6] An estimate of $N(E_F)$ may also be made from magnetic susceptibility measurements on KC_8.[26] The total susceptibility was found to be $\chi^c=138\times10^{-6}$ cm^3/mole. An estimate of the core diagmagnetic contribution to χ^c was given as $\chi^0=-52\times10^{-6}$ cm^3/mole, and the orbital susceptibility as obtained from a tight-binding-model calculation[27] was $\chi^{or}=73\times10^{-6}$ cm^3/mole for unit charge transfer. Using these estimates, the Pauli susceptibility may be extracted: $\chi_p=\chi^c-\chi^0-\chi^{or}=117\times10^{-6}$ cm^3/mole. This corresponds to $N(E_F)=0.45$ states/C atom eV, well above the value obtained from specific-heat measurements or from electronic structure calculations. Recent spin-susceptibility measurements on LiC_6 suggest[28] that the problem is that the calculated χ^{or} is too small by a factor of 2. Although this leads to a more reasonable prediction for $N(E_F)$, it is clear that susceptibility cannot presently provide a reliable prediction for the density of states in KC_8.

Measurements of the de Haas–van Alphen effect in KC_8 are quite difficult because of sample quality and the high frequency of the predicted extremal orbits. The one successful experiment[24] has observed a single frequency at 2.9×10^7 G. This is in reasonable agreement with either the extremal orbit frequencies reported here or the extremal orbit of the zone-edge piece of the Fermi surface of Inoshita *et al.*[6] Their calculation, unlike ours, predicts a number of lower frequencies which have

not been reported.

Several measurements of the visible and near-infrared reflectivity of KC_8 have been reported.[29,30] For $\vec{E}\perp c$, a high ($\simeq 95\%$) reflectivity is observed up to about 2.2 eV, then a sharp drop with a minimum at 2.5 eV. This, of course, supports the accepted view of KC_8 as a metal, and the plasma frequency obtained from a Drude fit to this reflectivity, $\omega_p = 3.5$ eV, is in rough agreement with the $\vec{E}\perp c$ plasma frequency calculated here, $\omega_a = 4.5$ eV. However, it was also found that a much better fit was obtained by including two Drude terms, suggesting that there are two different types of carriers in the KC_8 conduction bands. Similar Drude fits to reflectance measurements with $\vec{E}\|c$ suggest that one of these two types of carriers is rather isotropic. These conclusions, although model dependent, lead to a reasonable prediction of the small anisotropy of the electrical conductivity in KC_8 ($\sigma_a/\sigma_c \simeq 34$).[31] Therefore, reflectivity data lend strong support to a partially filled K s band as suggested by Inoshita and Ohno and co-workers. We believe that much more detailed and definitive information could be extracted from reflectivity measurements if the dielectric function could be obtained from Kramers-Kronig analysis.

The Hall coefficient is very small in KC_8 ($n_H = -1/R_H e = 7.8\times 10^{22}$ cm^{-3} at room temperature[30]), and it changes sign from n type to p type between room temperature and 4 K.[32] Since the Fermi surface of Inoshita *et al.* contains both hole and electron orbits from a free-electron model, it has been inferred that it is capable of explaining the Hall data, and that the rigid-band Fermi surface (or that of the present study), which contains only electron orbits, is not. However, taking into account the curvature of the Fermi surface, as is important at low fields, within a simple model,[33] the small value of R_H at low temperatures can be explained. In fact, a much more sophisticated analysis would be required to predict the T dependence of the Hall data.

Several independent electron energy-loss measurements have been performed on KC_8. Hwang and co-workers[34] have measured the electron energy-loss (EEL) spectrum up to 40 eV, and have extracted the loss function and dielectric function. The resulting $\epsilon_2(\omega)$ shows that the strong interband transition at 4.5 eV at the M point still appears in KC_8, but is shifted down to about 3.8 eV and broadened. As we have remarked previously,[35] and as shown in Table II, this structure at 3.8 eV can be identified successfully with a set of interband

TABLE II. Optical selection rules and principle low-energy critical-point transitions at the Γ point in KC_8.

Optical selection rules at Γ	
$1+\overset{\parallel}{\leftrightarrow}3-$	$2+\overset{\perp}{\leftrightarrow}1-$
$1+\overset{\parallel}{\leftrightarrow}4-$	$4+\overset{\parallel}{\leftrightarrow}2-$
$1+\overset{\perp}{\leftrightarrow}2-$	$4+\overset{\parallel}{\leftrightarrow}1-$
$3+\overset{\parallel}{\leftrightarrow}1-$	$4+\overset{\perp}{\leftrightarrow}3-$
$3+\overset{\parallel}{\leftrightarrow}2-$	$2+\overset{\parallel}{\leftrightarrow}4-$
$3+\overset{\perp}{\leftrightarrow}4-$	$2+\overset{\parallel}{\leftrightarrow}3-$
Transition at Γ	**ΔE (eV)**
$4-\rightarrow 2+$	3.4
$4-\rightarrow 1+$	3.5
$3-\rightarrow 2+$	3.5
$4+\rightarrow 1-$	3.8
$3+\rightarrow 1+$	3.9
$3+\rightarrow 1-$	4.1
$4+\rightarrow 1-$	4.2
$3+\rightarrow 2-$	4.3
$4+\rightarrow 2-$	4.5
$3-\rightarrow 2+$	4.7
$4-\rightarrow 2+$	4.8

critical transitions at Γ in our KC_8 band structure. Recent EEL measurements by Ritsko[36] have also provided loss function and dielectric constant data for 0.2–300 eV. In these experiments the core excitation spectrum of C 1s electrons has been used to probe the nature of states near the Fermi level. These spectra are found to be much more complex for KC_8 than for LiC_6. Since LiC_6 is agreed to have only C π states at the Fermi level, it has been argued that KC_8 must therefore have metal s states at the Fermi level resulting either from a partially occupied K band or π-s hybridization. This conclusion cannot be considered firm, however, until the effect of the core exciton[37] is accounted for. In any case, the interpretation of both EEL experiments would be greatly aided by a theoretical calculation of the dielectric function from the band structure.

Oelhafen and co-workers have performed a careful systematic study of ultraviolet photoemission spectroscopy (UPS) spectra for the alkali-metal–intercalation compounds.[38] The shape of their photoemission spectrum near the Fermi energy for KC_8 is similar to the density of states presented here. However, their analysis of the shape of the spectra as a function of the exciting photon energy provides a strong indication that K s states lie below E_F. They have also supported this

view with positron annihilation studies.[39] Still, a similar UPS analysis, which they have performed on second-stage potassium graphite KC_{24}, also indicates that only partial charge transfer has occurred. This is in disagreement with the interpretation of a polarized reflectance measurement on KC_{24} by Zanini and Fischer,[29] which implies that there has been full charge transfer from the K layer.

So, it appears that, while the evidence provided by experiments on KC_8 is not conclusive, it is necessary to consider the possibility that charge transfer from the potassium layers is not complete, and that states with K s character exist close to the Fermi level. Since the present calculation does not predict partial charge transfer we must understand why it does not and whether our conclusions could be affected by any of the approximations of our calculation. In fact, there is evidence that if the approximations made for the crystal potential in the present calculation could be lifted, then the topology of the Fermi surface and the nature of the Fermi-level states could be modified. This evidence is provided by a new calculation[40] for LiC_6 using a self-consistent potential and with the Hedin-Lundqvist local approximation to the exchange and correlation potential. Previous theoretical work[5,41] on LiC_6 used a non-self-consistent potential with $X\alpha$ exchange and correlation as in the present paper. Comparing the two different calculations on lithium graphite shows that the minimum of the metal s band is about 1 eV lower in the new work than in the original KKR calculation. Although a similar self-consistent-field calculation for KC_8 has not been completed, presumably the K 4s band will also be lower when self-consistency and different exchange and correlation are used. If the metal band lies closer to the Fermi level, it may be expected to hybridize more with states at the Fermi energy. Moreover, since the π bands are very flat at E_F, any distortions of the bands due to hybridization could have large effects on the shape of the Fermi surface. A further lowering of the Γ_2^+ level lying at the Fermi level, for example, could introduce a new portion of the Fermi surface at Γ, changing the topology of the Fermi surface.

Despite these possible difficulties, our calculation should be judged successful on several points. The validity of the rigid-band model as a global description of the filled valence bands of first-stage potassium graphite has been established. At the same time, it has been demonstrated that small deviations from the rigid-band model near the Fermi level can lead to both qualitative and quantitative deviation from the rigid-band predictions. The present calculation predicts for the first time the position of the K 3p core states with respect to the Fermi level, and confirms the picture of the K 4s band as isotropic and free-electron-like. For the theoretician, our calculation provides another demonstration that modified muffin-tin techniques of band calculation can be used successfully for highly anisotropic materials.

Note added in proof. Recent work on KC_8 by Ritsko and Brucker[48] combining EEL and UPS measurements suggest a peak in the K s density of states of 2.0—2.5 eV above E_F, in good agreement with the present calculation.

ACKNOWLEDGMENTS

We thank Robert C. Tatar and Natalie Holzwarth for their constant interest in this work, for their help in performing the calculations, and for their critical reading of this manuscript. Thanks also to John E. Fischer and the graphite group at Penn for many stimulating discussions. We are grateful to the Moore School Computing Facility for the use of their Univac 90/70 computer. This work was supported by the NSF, MRL program under Grant No. DRM-7923647, by ARO Contract No. DAAG/29/80/K/0019, and by the IBM predoctoral fellowship program.

APPENDIX A: MODIFIED KKR FORMALISM

In this appendix we present the expressions used to evaluate the KKR secular matrix, Eq. (1). The Hamiltonian matrix elements $\mathcal{K}^{-1}$ and M are straightforward extensions of what has appeared in the literature,[16,42] generalized for many atoms per unit cell and for nonspherical muffin-tin potentials.

$\mathcal{K}^{-1}(E)$, the KKR scattering or reaction matrix, measures the strength of scattering of partial waves of energy E at the muffin-tin boundary. It is given by the expression

$$\mathcal{K}^{-1}(E)^{\vec{\tau}}_{lml'm'} = \sum_{LM} [\mathcal{N}^{-1}]^{\vec{\tau}}_{LM,lm} \mathcal{J}^{\vec{\tau}}_{l'm',LM} , \tag{A1}$$

where

$$\mathcal{N}^{\vec{\tau}}_{LM,lm}=\left[R^{\vec{\tau}}_{LM,lm}(E,\vec{r})\frac{dn_l(\kappa r)}{dr}-\frac{dR^{\vec{\tau}}_{LMlm}(E,\vec{r})}{dr}n_L(\kappa r)\right]\kappa r^2\Bigg|_{r=r^{\vec{\tau}}_{\rm MT}}, \tag{A2}$$

and

$$\mathcal{J}^{\vec{\tau}}_{l'm'LM}=\left[R^{\vec{\tau}}_{l'm'LM}(E,\vec{r})\frac{dj_L(\kappa r)}{dr}-\frac{dR^{\vec{\tau}}_{l'm'LM}(E,\vec{r})}{dr}j_{l'}(\kappa r)\right]\kappa r^2\Bigg|_{r=r^{\vec{\tau}}_{\rm MT}}. \tag{A3}$$

$n_l(\kappa r)$ is the Neuman function, $j_l(\kappa r)$ is the spherical Bessel function, and $R^{\vec{\tau}}_{lmLM}(E,\vec{r})$ is the solution to the radial Schrödinger equation at site $\vec{\tau}$:

$$\sum_{l,m}\left\{\delta_{ll'}\delta_{mm'}\left[-\frac{\hbar^2}{2m}\frac{d^2}{dr^2}[rR^{\vec{\tau}}_{lml'm'}(E,\vec{r})]+\left[\frac{\hbar^2 l(l+1)}{r^2}-E\right]rR^{\vec{\tau}}_{lml'm'}(E,\vec{r})\right]\right.$$
$$\left.+rR^{\vec{\tau}}_{lml'm'}(E,\vec{r})\int Y^*_{l'm'}(\hat{r})V_{\rm cryst}(\vec{r})Y_{lm}(\hat{r})\hat{d}r\right\}=0. \tag{A4}$$

$\hat{d}r$ indicates an angular integral about site $\vec{\tau}$. We solve (A4) for $l\leq 2$ by the Noumerov technique.[43,44] Full use of group theory is made, so that (A4) is evaluated for the minimum number of different sites $\vec{\tau}$, and for the minimal set l,m,l',m' (see Appendix C).

The structure matrix $M(\vec{k},E)$ is a purely geometrical quantity which describes the projection of a partial wave at site $\vec{\tau}$ onto another partial wave at another site $\vec{\tau}'$. It is given by

$$M^{\tau\tau'}_{lml'm'}(\vec{k},E)=\sum_{\vec{T}}{}' e^{i\vec{k}\cdot(\vec{\tau}'-\vec{\tau}+\vec{T})}N_{lml'm'}(\vec{\tau}-\vec{\tau}'-\vec{T}), \tag{A5}$$

where $\vec{T}$ is a real lattice vector, and the prime indicates the exclusion of the $T=0$ term. $N_{lml'm'}$ is given by

$$N_{lml'm'}(\vec{r})=4\pi i^{(l-l')}\sum_{LM}i^{-L}n_L(\kappa r)Y^*_{LM}(\hat{r})\int Y^*_{lm}(\hat{r}')Y_{LM}(\hat{r}')Y_{l'm'}(\hat{r}')\hat{d}r'. \tag{A6}$$

κ is the scalar wave vector $(2m|E|/\hbar^2)^{1/2}$ and n_L is again the Neumann function. In practice, the real space sum in (A5) converges too slowly for practical calculations. We therefore apply the Ewald procedure[16] to (A5), transferring part of the sum into reciprocal space. The result is

$$M^{\vec{\tau}\vec{\tau}'}_{lml'm'}=-4\pi i^{(l-l')}\sum_{L,M}i^{-L}(\mathcal{R}^{\vec{\tau}\vec{\tau}'(1)}_{LM}+\mathcal{R}^{\vec{\tau}\vec{\tau}'(2)}_{LM}+\mathcal{R}^{\vec{\tau}\vec{\tau}'(3)}_{LM})C^{LM}_{lml'm'}, \tag{A7}$$

where

$$\mathcal{R}^{\vec{\tau}\vec{\tau}'(1)}_{LM}=\frac{4\pi i^L}{V_{\rm UC}\kappa^{L+1}}\sum_{\vec{G}}e^{i(\vec{k}+\vec{G})\cdot(\vec{\tau}-\vec{\tau}')}Y^*_{LM}\left[\frac{\vec{k}+\vec{G}}{|\vec{k}+\vec{G}|}\right]\frac{(\vec{k}+\vec{G})^2e^{[E-(\vec{k}+\vec{G})^2]/\eta}}{(\vec{k}+\vec{G})^2-E}, \tag{A8}$$

$$\mathcal{R}^{\vec{\tau}\vec{\tau}'(2)}_{LM}=\frac{1}{\sqrt{4\pi}}\left[\frac{\kappa}{2}\right]^L\sum_{\vec{T}}{}'|\vec{\tau}-\vec{\tau}'+\vec{T}|Y^*_{LM}\left[\frac{\vec{\tau}-\vec{\tau}'+\vec{T}}{|\vec{\tau}-\vec{\tau}'+\vec{T}|}\right]e^{i\vec{k}\cdot\vec{T}}$$
$$\times\frac{1}{\sqrt{\pi}}\left[\frac{E}{4}\right]^{L+\frac{1}{2}}\int_0^{E/\eta}u^{-3/2-L}e^{u-E(\vec{\tau}'-\vec{\tau}+\vec{T})^2/4u}du, \tag{A9}$$

$$\mathcal{R}^{\vec{\tau}\vec{\tau}'(3)}_{LM}=\frac{\sqrt{\eta}}{2\pi\kappa}\sum_{n=0}^{\infty}\frac{1}{n!(2n-1)}\delta_{\vec{\tau}\vec{\tau}'}\delta_{L0}\delta_{M0}, \tag{A10}$$

and

$$C^{LM}_{lml'm'}=\int\hat{d}r'Y^*_{lm}(\hat{r}')Y_{LM}(\hat{r}')Y_{l'm'}(\hat{r}'). \tag{A11}$$

$V_{\rm UC}$ is the volume of the real-space unit cell. For $\eta=0.22$, the sums converge in a few hundred terms, which is quite practical for actual calculations. The KKR eigenvalues are given by the roots of the equation

$$\det[\mathcal{A}^{-1}(E_{\rm eig})+M(\vec{k},E_{\rm eig})]=0\ . \tag{A12}$$

We show the resulting $E_{\rm eig}(\vec{k})$ in Fig. 9. This 82×82 determinant can often be blocked diagonalized by using symmetry (see Appendix C).

The eigenvectors of the secular matrix at the energies $E_{\rm eig}$, $w_{lm}^{\vec{\tau}}$, give the KKR wave functions within the interstitial region:

$$\Psi_n^{\rm KKR}(\vec{k},\vec{r})=\sum_{\vec{\tau},l,m} w_{nlm}^{\vec{\tau}} \sum_{\vec{T}} e^{i\vec{k}\cdot(\vec{\tau}+\vec{T})}\left[-n(\kappa|\vec{r}-\vec{\tau}-\vec{T}|)Y_{lm}\left[\frac{\vec{r}-\vec{\tau}-\vec{T}}{|\vec{r}-\vec{\tau}-\vec{T}|}\right]\right]. \tag{A13}$$

Again, a more rapidly convergent expression is obtained using a Ewald decomposition:

$$\begin{aligned}\Psi_n^{\rm KKR}(\vec{k},\vec{r})=&\frac{4\pi}{V_{\rm UC}\kappa}\sum_{\vec{G}} e^{i(\vec{k}+\vec{G})\cdot\vec{r}}\frac{\exp\{[\kappa^2-(\vec{k}+\vec{G})^2]/\eta\}}{(\vec{k}+\vec{G})^2-\kappa^2}\sum_{\vec{\tau},l,m} i^{-l}e^{-i\vec{G}\cdot\vec{\tau}}\left[\frac{|\vec{k}+\vec{G}|}{\kappa}\right]^l Y_{lm}\left[\frac{\vec{k}+\vec{G}}{|\vec{k}+\vec{G}|}\right]w_{nlm}^{\vec{\tau}}\\&+\frac{1}{4\pi}\sum_{\vec{T},\vec{\tau},l,m} e^{i\vec{k}\cdot(\vec{\tau}+\vec{T})}\int_0^{\kappa^2/\eta}\exp\left[u-\frac{u^2|\vec{r}-\vec{\tau}-\vec{T}|^2}{4u}\right]u^{-3/2-l}du\\&\times\left[\frac{\kappa|\vec{r}-\vec{\tau}-\vec{T})}{2}\right]^l Y_{lm}\left[\frac{\vec{r}-\vec{\tau}-\vec{T}}{|\vec{r}-\vec{\tau}-\vec{T}|}\right]w_{nlm}^{\vec{\tau}}\ .\end{aligned} \tag{A14}$$

An Ewald parameter of $\eta=0.8$ was found to give the best results. Equation (A14) provides a starting point for the calculation of the matrix elements of ΔV (Appendix B).

APPENDIX B: CALCULATION OF NON-MUFFIN-TIN CORRECTIONS

In this appendix we give the details of the evaluation of the matrix element of the residual crystal potential $\Delta V(r)$ between KKR wave functions $\Psi_n^{\rm KKR}(\vec{k},\vec{r})$. The calculation of the KKR wave functions is outlined in Appendix A, and $\Delta V(\vec{r})$ is determined by subtracting the constant muffin-tin potential $V_{\rm MT}$ from the model crystal potential $V_{\rm cryst}(\vec{r})$ in the interstitial region. Because of the symmetry of the wave vectors,[18] we were able to do the integral of Eq. (3) in $\frac{1}{8}$ or at most $\frac{1}{4}$ of the unit cell (see Appendix C). Also, since $\Delta V(\vec{r})$ is zero within the muffin tins, the integral is restricted to the interstitial region. This is not much of an advantage, because, as Fig. 10 shows, this integration region is highly irregular.

We adopted a very straightforward procedure for evaluating $\Delta_{nn'}$; we approximated Eq. (3) by

$$\Delta_{nn'}(\vec{k})=\sum_i w_i\Psi_n^{\rm KKR*}(\vec{k},\vec{r}_i)\Delta V(\vec{r})\Psi_{n'}^{\rm KKR}(\vec{k},\vec{r}_i)\ , \tag{B1}$$

where w_i are the weights of the integration points r_i. These points are chosen using a one-dimensional Gaussian quadrature algorithm[45] applied successively in the three coordinate directions; that is,

$$\int f(\vec{r})d\vec{r}\simeq\sum_i w_i^x\left[\sum_i w_j^y\left[\sum_k w_k^z f(x_i,y_j,z_k)\right]\right]. \tag{B2}$$

$w_i^{x,y,z}$ is the one-dimensional Gaussian weight. The one-dimensional integration regions of (B2) were chosen carefully so as to avoid discontinuities resulting from the irregular geometry of the integration region. The interested reader should see Ref. 43 for details. Grids containing up to 6000 points were tested, and from these tests it was determined that a grid of 1675 points provides adequate convergence for all the relevant matrix elements $\Delta_{nn'}(\vec{k})$.

APPENDIX C: SYMMETRIZATION

In this appendix we discuss the uses of symmetry in our calculation. Symmetry naturally is indispensible in sorting out our results and in revealing their physical significance. On a more practical level, it helps to reduce the extremely lengthy

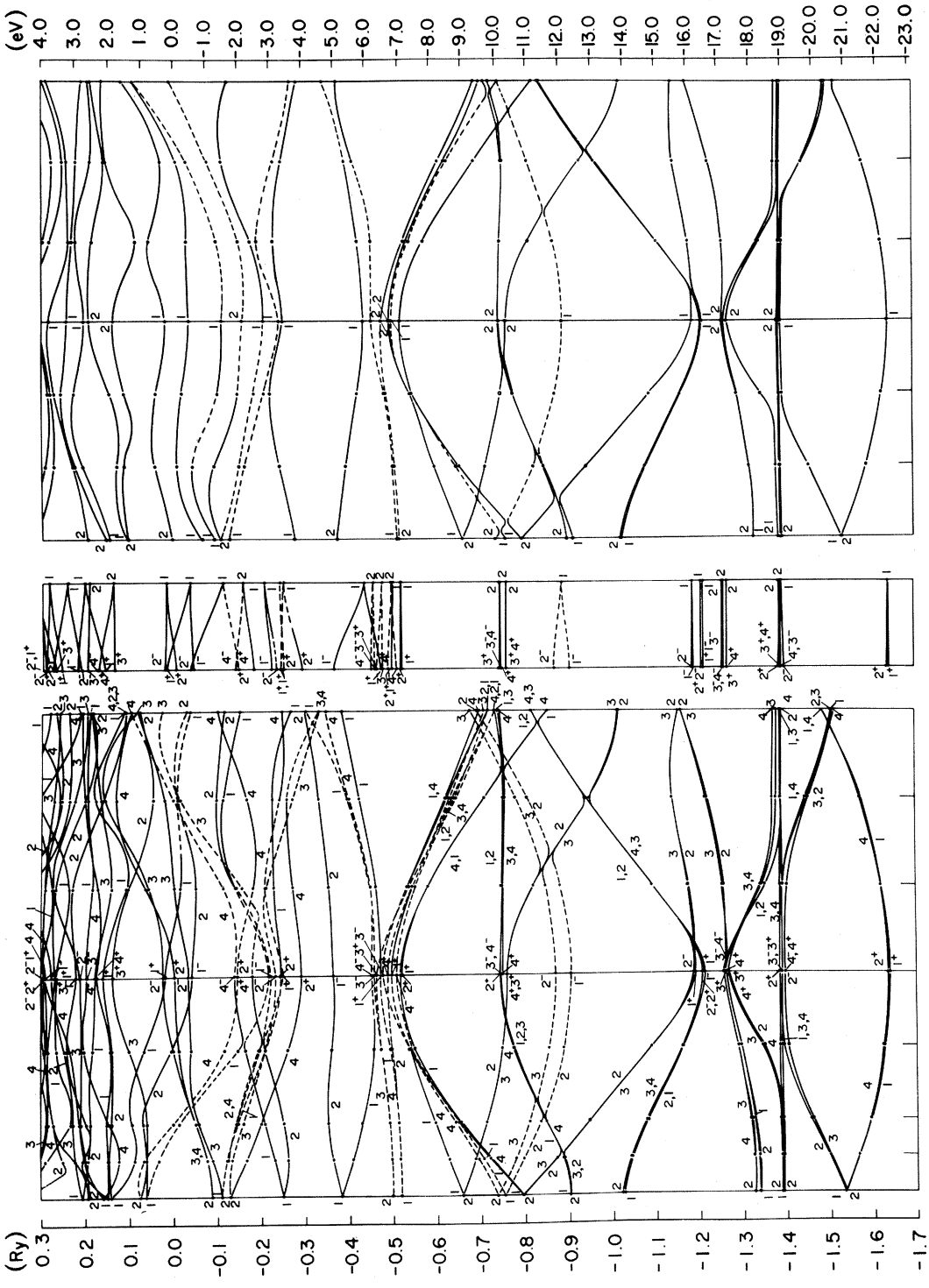

FIG. 9. KKR energy bands of KC_8 in the muffin-tin approximation. The π bands are shown as dashed lines, σ bands are solid lines. Note the inaccurate position of the K 4s band (Γ_1^+ at -6.5 eV) within this approximation.

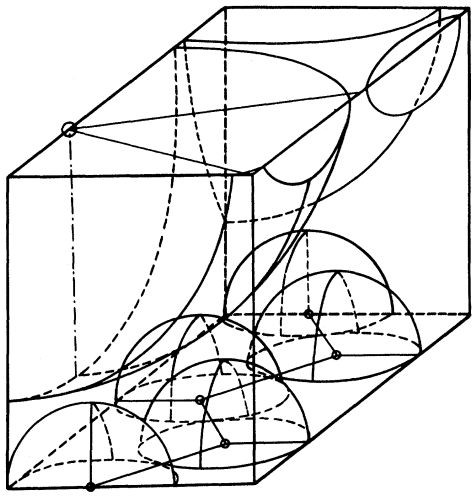

FIG. 10. The irreducible sector ($\frac{1}{8}$) of the KC_8 unit cell. The carbon and potassium muffin tins are shown. Note the irregularity of the interstitial volume, in which the integral for $\Delta_{nm}(\vec{k})$ must be performed.

numerical calculations required for our work. Most of the computer time is spent in the evaluation of matrix elements. Group theory tells us the smallest possible set of matrix elements which must be evaluated. When the matrix element is given by a sum or integral, group theory also gives us the smallest possible domain over which that sum or integral must be performed. These two applications of group theory make the KC_8 band-structure calculation tractible.

We now give several specific uses of symmetry properties in our work. The determination of the KKR scattering matrix (see Appendix A) requires the evaluation of the integral [see Eq. (A4)]

$$\int Y^*_{l'm'}(\hat{r}_{\vec{\tau}})V_{\text{cryst}}(\hat{r}_{\vec{\tau}})Y_{lm}(\hat{r}_{\vec{\tau}})d\hat{r}_{\vec{\tau}} \qquad \text{(C1)}$$

on a sphere of radius $|\vec{r}_{\vec{\tau}}|$ for every site $\vec{\tau}$. First, the symmetry of the crystal is such that there are only three inequivalent sites in the crystal, two C sites and one K site; therefore, (C1) needs to be evaluated for just three values of $\vec{\tau}$. Further simplifications result from the point-group symmetry about each site $\vec{\tau}$. In KC_8, C sites are not at centers of symmetry, so no further reduction is possible. The point-group symmetry at K is D_2, which is of considerable value in doing the integral. Since D_2 has four group elements, the spherical integral needs to be evaluated only on $\frac{1}{4}$ of the surface of the sphere. Other properties of D_2 permit us to reduce the number of integrals calculated. Since we consider partial wave scattering up to $l=2$, Eq. (C1) represents

$$81=\left[\sum_{l=0}^{2}(2l+1)\right]^2$$

integrals. Because of symmetry, many of these 81 are zero, and many are related to others. We proceed by replacing the spherical harmonics by spherical polynomials which transform according to the irreducible representations of D_2.[46] These polynomials are exhaustively catalogued by Bell.[47] Using this procedure, we reduce the number of integrals required from 81 to 9, and we block diagonalize the 9×9 matrix into four blocks of dimensions 2, 2, 2, and 3. These simplifications improve the accuracy and speed of the calculation of the KKR scattering matrix considerably.

An application of the space-group symmetry leads to a block diagonalization of the KKR secular matrix. The terms of Eq. (1) may be looked upon as matrix elements of the KKR Hamiltonian between KKR basis functions:

$$\mathcal{K}^{-1}(E)^{\vec{\tau}}_{lml'm'}\delta_{\vec{\tau}\vec{\tau}'}+M(\vec{k},E)^{\vec{\tau}\vec{\tau}'}_{lml'm'}=\langle\phi^{\text{KKR}\,\vec{\tau}}_{l'm'}\,|\,H_{\text{KKR}}\,|\,\phi^{\text{KKR}\,\vec{\tau}'}_{lm}\rangle\ , \qquad \text{(C2)}$$

where the KKR basis functions are those implicit in Eqs. (A13):

$$\phi^{\text{KKR}\,\vec{\tau}}_{lm}(\vec{k},\vec{r})=\sum_{\vec{T}}e^{i\vec{k}\cdot(\vec{\tau}+\vec{T})}\left[-n_l(\kappa\,|\,\vec{r}-\vec{\tau}-\vec{T}\,|\,)Y_{lm}\left[\frac{\vec{r}-\vec{\tau}-\vec{T}}{|\,\vec{r}-\vec{\tau}-\vec{T}\,|}\right]\right]. \qquad \text{(C3)}$$

This treatment is somewhat schematic; although (C3) is not actually the basis function used for the KKR matrix elements, it displays all the symmetry properties necessary for this discussion.

For high-symmetry points, we can block diagonalize (C2) by applying to the wave functions $\phi^{\text{KKR}\,\vec{\tau}}_{lm}$ a projection operator for an irreducible representation of the group of $\vec{k}$ (Ref. 43):

$$\phi_{\text{sym}}^{\Gamma_i(\vec{k})}(\vec{r}) = \sum_{(\beta|\vec{b})\in G(\vec{k})} D_{mm}^{\Gamma_i(\vec{k})}[(\beta|\vec{b})] \times[(\beta|\vec{b})\phi_{lm}^{\text{KKR}\,\vec{\tau}}(\vec{k},\vec{r})] , \tag{C4}$$

where $D_{mm}^{\Gamma_i(\vec{k})}(\beta|\vec{b})$ is the mm element of the matrix representing crystal symmetry operation $(\beta|\vec{b})$ in irreducible representation $\Gamma_i(\vec{k})$; these are all given in Ref. 18. Details of the actual projection on the functions (C3) are given in Ref. 43. When the KKR Hamiltonian is expressed in the symmetrized basis (C3), the matrix is block diagonalized, making the diagonalization more rapid, and eigenvalues and eigenvectors more reliable.

As a final example of the application of symmetry to our calculation, we mention the simplifications which can be made in the matrix elements of ΔV, the non-muffin-tin part of the potential [see Eq. (3)]. First, because $\Delta V(r)$ transforms according to the identity representation of the crystal group, there are nonzero matrix elements only between those KKR wave functions n and n', which transform according to the same irreducible representations. This property of ΔV also tells us that degenerate KKR eigenvalues are not split by the perturbation.

In addition to these selection rules, symmetry allows us to reduce the region of integration in (B1). The integrand is invariant under every symmetry operation of the group of $\vec{k}$. Consequently, if the order of the group is g_k, then the integral need only be done over $1/g_k$ of the unit cell. For KC_8, this means $\frac{1}{8}$ of the unit cell for wave vectors Γ, X, Y, Z, Σ, Δ, and Λ, and $\frac{1}{4}$ of the unit cell for wave vectors A and B (see Fig. 3).

[1]J. E. Fischer and T. E. Thompson, Phys. Today 31, (7), 36 (1978).

[2]Proceedings of the Franco-American Conference on Intercalated Compounds of Graphite, edited by F. L. Vogel and A. Herold [Mater. Sci. Eng. 31, (1977)].

[3]Proceedings of the International Conference on Layered Materials and Intercalates, edited by C. F. van Bruggen, C. Haas, and H. W. Myron [Physica B 99, (1980)].

[4]Second Conference on Intercalation Compounds of Graphite, edited by F. L. Vogel [Synth. Metals 2, (1980)].

[5]N. A. W. Holzwarth, S. Rabii, and L. A. Girifalco, Phys. Rev. B 18, 5190 (1978).

[6]T. Inoshita, K. Nakao, and H. Kamimura, J. Phys. Soc. Jpn. 43, 1237 (1977); 45, 689 (1978).

[7]T. Ohno, K. Nakao, and H. Kamimura, J. Phys. Soc. Jpn. 47, 1125 (1979).

[8]W. Rudorff, and E. Schultze, Z. Anorg. Chem. 277, 156 (1954).

[9]P. LaGrange, D. Guerard, and A. Herold, Ann. Chim. (Paris) 3, 143 (1978).

[10]C. Horie, M. Maeda, and Y. Kuramoto, Physica B 99, 430 (1980).

[11]*International Tables of X-Ray Crytallography* (Kynoch, Birmingham, 1952), p. 161.

[12]J. C. Slater, *The Self-Consistent Field for Molecules and Solids* (McGraw-Hill, New York, 1974).

[13]K. Schwartz, Phys. Rev. B 5, 2466 (1972).

[14]F. Herman and S. Skillman, *Atomic Structure Calculations* (Prentice-Hall, Englewood Cliffs, N.J., 1963).

[15]J. Korringa, Physica (Utrecht) 13, 392 (1947); W. Kohn and N. Rostoker, Phys. Rev. 94, 1111 (1954).

[16]F. S. Ham and B. Segall, Phys. Rev. 124, 1786 (1961).

[17]G. S. Painter, Phys. Rev. B 7, 3520 (1973).

[18]S. C. Miller and W. F. Love, *Tables of Irreducible Representations of Magnetic Space Groups and Co-Representations of Magnetic Space Groups* (Pruett, Boulder, Colo., 1967).

[19]H. Nagayoshi, K. Nakao, and Y. Uemura, J. Phys. Soc. Jpn. 41, 2480 (1976).

[20]J. C. Slater and G. F. Koster, Phys. Rev. 94, 1498 (1954).

[21]R. C. Tatar, following paper, Phys. Rev. B 25, 4126 (1982).

[22]T. Kondow, U. Mizutani, and T. B. Massalski, Mater. Sci. Eng. 31, 267 (1977).

[23]A. V. Gold, in *Solid State Physics, Electrons in Metals,* edited by J. F. Cochran and R. R. Haering (Gordon and Breach, New York, 1968), p. 39.

[24]H. Suematsu, S. Tanuma, and K. Higuchi, Physica B 99, 420 (1980).

[25]N. F. Mott and H. Jones, *The Theory of the Properties of Metals and Alloys* (Dover, New York, 1958), p. 96.

[26]F. J. DiSalvo, S. A. Safran, R. C. Haddon, J. V. Waszczak, and J. E. Fischer, Phys. Rev. B 20, 4883 (1979).

[27]S. A. Safran and F. J. DiSalvo, Phys. Rev. B 20, 4889 (1979).

[28]J. E. Fischer, private communication.

[29]M. Zanini and J. E. Fischer, Mater. Sci. Eng. 31, 169 (1977).

[30]D. Guerarad, G. M. T. Foley, M. Zanini, and J. E. Fischer, Nuovo Cimento 38, 410 (1977).

[31]A. R. Ubbelohde, Nature 232, 43 (1971); C. D. Fuerst, W. D. Johnson, and J. E. Fischer, Extended Abstracts and Program of the 14th Biennial Conference on Carbon, 1979 (unpublished), p. 296.

[32]W. D. Johnson, M. E. Potter, and J. E. Fischer, Bull. Am. Phys. Soc. 24, 410 (1979).
[33]N. A. W. Holzwarth, Phys. Rev. B 21, 3665 (1980).
[34]D. M. Hwang, M. Utlaut, M. S. Isaacson, and S. A. Solin, Physica B 99, 435 (1980).
[35]D. P. DiVincenzo, N. A. W. Holzwarth, and S. Rabii, Synth. Metals 3, 125 (1981).
[36]J. J. Ritsko, Bull. Am. Phys. Soc. 26, 264 (1981).
[37]E. Mele (private communication).
[38]P. Oelhafen, P. Pfluger, E. Hanser, and H. J. Güntherodt, Phys. Rev. Lett. 44, 197 (1980); J. Krieg, P. Oelhafen, P. Pfluger, and H. J. Güntherodt, in Extended Abstracts and Program, 15th Biennial Conference on Carbon, 1981 (unpublished), p. 84.
[39]E. Cartier, F. Heinrich, P. Pfluger, and H. J. Güntherodt, Phys. Rev. Lett, 46, 272 (1981); Extended Abstracts and Program, 15th Biennial Conference on Carbon, 1981 (unpublished), p. 86.
[40]N. A. W. Holzwarth, Bull. Am. Phys. Soc. 26, 450 (1981), and unpublished.
[41]N. A. W. Holzwarth, L. A. Girifalco, and S. Rabii, Phys. Rev. B 18, 5206 (1978).
[42]W. John, G. Lehmann, and P. Ziesche, Phys. Status Solidi B 53, 287 (1972); B. Segall, J. Phys. Chem. Solids 8, 371 (1959).
[43]D. P. DiVincenzo, Master's thesis, University of Pennsylvania, 1980 (unpublished).
[44]D. R. Hartree, *Numerical Analysis* (Oxford University Press, London, 1958), p. 142.
[45]F. B. Hildebrand, *Introduction to Numerical Analysis* (McGraw-Hill, New York, 1974), p. 379.
[46]M. Tinkham, *Group Theory and Quantum Mechanics* (McGraw-Hill, New York, 1964).
[47]D. G. Bell, Rev. Mod. Phys. 26, 311 (1954).
[48]J. J. Ritsko and C. F. Brucker, Bull. Am. Phys. Soc. 27, 405 (1982), and unpublished.